Journal of Power Sources 214 (2012) 91–99

Contents lists available at SciVerse ScienceDirect

Journal of Power Sources

journal homepage: www.elsevier.com/locate/jpowsour

Synthesis of Co_3O_4 nanosheets via electrodeposition followed by ozone treatment and their application to high-performance supercapacitors

Chung-Wei Kung [a], Hsin-Wei Chen [a], Chia-Yu Lin [a], R. Vittal [a], Kuo-Chuan Ho [a,b,*]

[a] Department of Chemical Engineering, National Taiwan University, Taipei 10617, Taiwan
[b] Institute of Polymer Science and Engineering, National Taiwan University, Taipei 10617, Taiwan

HIGHLIGHTS

- Thin film of $Co(OH)_2$ nanosheets is converted to Co_3O_4 by UV–ozone treatment.
- Synthesis of Co_3O_4 film is done at low temperature on flexible substrate.
- The specific capacitance of the film after UV–ozone treatment reaches 1033.3 F g^{-1}.
- The capacitance is more than 10 times higher than the film before the treatment.
- Still 77% of specific capacitance remains after 3000 cycles of charge/discharge.

ARTICLE INFO

Article history:
Received 28 December 2011
Received in revised form
28 March 2012
Accepted 26 April 2012
Available online 3 May 2012

Keywords:
Capacitor performance
Charge–discharge current density
Cobalt oxide
Electrodeposition
Flexible supercapacitor
UV–ozone treatment

ABSTRACT

A thin film of Co_3O_4 nanosheets is electrodeposited on a flexible Ti substrate by a one-step potentiostatic method, followed by an UV–ozone treatment for 30 min. The films before and after the UV–ozone treatment are characterized with X-ray diffraction (XRD) and X-ray photoelectron spectroscopy (XPS). The film is composed of $Co(OH)_2$ before UV–ozone treatment, and of Co_3O_4 after the treatment. The morphologies of both films are examined by scanning electron microscopy (SEM) and transmission electron microscope (TEM). The obtained films are composed of nanosheets, and there is no change in their sheet-like morphology before and after the UV–ozone treatment. When applied for a supercapacitor, the Co_3O_4 modified Ti electrode (Co_3O_4/Ti) shows a far higher capacitance than that of the $Co(OH)_2$ modified Ti electrode. The electrodeposition time and NaOH concentration in the electrolyte are optimized. A remarkably high specific capacitance of 1033.3 F g^{-1} is obtained for the Co_3O_4 thin film at a charge–discharge current density of 2.5 A g^{-1}. The long-term stability data shows that there is still 77% of specific capacitance remaining after 3000 repeated charge–discharge cycles. The high specific capacitance and long-term stability suggest the potential use of Co_3O_4/Ti for making a flexible supercapacitor.

© 2012 Elsevier B.V. All rights reserved.

1. Introduction

Energy storage is one of the major challenges in recent years due to the fast-growing demand for high-performance energy storage devices for consumer electronics, electric vehicles, and medical electronics [1]. Among several kinds of energy storage devices, electrochemical capacitors (supercapacitors) became eye-catching, because of their high power density, high energy efficiency, and long charge–discharge cycle life [2]. Supercapacitors can be classified into two categories, electrochemical double-layer capacitors (EDLCs) and electrochemical pseudocapacitors (EPCs), depending on their energy storage mechanism. An electrochemical double-layer capacitor (EDLC) is usually based on the capacitance of one of its electrodes (with or without a film) arising due to the charge separation at this electrode/electrolyte interface. An electrochemical pseudocapacitor (EPCs) is usually based on the capacitance of one of its electrodes arising from fast and reversible faradic redox reactions within the electroactive material on this electrode. Much attention has been paid on the EPCs, in recent years, due to their superior energy density than that of EDLCs [3]. Several metal oxides, e.g., RuO_2 [4], MnO_2 [5], and NiO [6] have been investigated as the electrode materials for pseudocapacitors. Among these, Co_3O_4 has attracted considerable interest in the field of pseudocapacitors, due to its excellent redox activity and environmental friendliness [2]. The theoretical specific capacitance of Co_3O_4 is 3560 F g^{-1} [2]. Besides, the nano-scale morphology of Co_3O_4 thin film is known to affect its redox activity in a significant way [7].

* Corresponding author. Postal address: No.1, Sec. 4, Roosevelt Rd., Da'an Dist., Taipei City 10617, Taiwan. Tel.: +886 2 2366 0739; fax: +886 2 2362 3040.
E-mail address: kcho@ntu.edu.tw (K.-C. Ho).

0378-7753/$ – see front matter © 2012 Elsevier B.V. All rights reserved.
doi:10.1016/j.jpowsour.2012.04.076

In order to obtain a high specific capacitance for a Co_3O_4 thin film in a pseudocapacitor, various Co_3O_4 nanostructures, e.g., nanotubes [3], nanowires [2], nanoparticles [8], and nanosheets [1] have been investigated. Recently, Qing et al. synthesized a film of Co_3O_4 nanoflowers on a Ni foam substrate by solvothermal method, and achieved a remarkably high specific capacitance of 1936.7 F g^{-1} [9] for its capacitor. In most of the works on Co_3O_4 based EPCs, calcination or annealing process was used to prepare Co_3O_4 thin films, which is energy-consuming and unsuitable in the case of several kinds of flexible substrates. Lightweight and flexible capacitors have advantages of easy transportation and roll-to-roll production, which makes them cost-effective. It is important to develop a simple and low-temperature process to prepare thin films of Co_3O_4 on flexible substrates.

UV–ozone treatment has been applied for several decades for surface cleaning of substrates or thin films [10]. The short-wavelength UV light can efficiently decompose O_2 in the air to produce ozone, and both the UV light and the produced ozone gas play important roles in the removal of the contaminant molecules on the surface of substrates or films [11]. Besides, due to strong oxidative ability of O_3 towards organics, the convenient vapor treatment is used for the removal of organic layers on the surfaces of nanostructures [12]. In addition to the applications for surface cleaning and removing of organics, the UV–ozone treatment is utilized to functionalize carbon nanotubes and carbon black; this way of functionalization is convenient and milder, with reference to the conventional way of functionalization by oxidative treatment, using acidic vapors or strong oxidants [13,14].

In this study, a thin film of cobalt oxide nanosheets was synthesized on a flexible Ti foil, first by a one-step, fast electrodeposition of a film, and then by an UV–ozone treatment to the electrodeposited film. An excellent specific capacitance of 1033.3 F g^{-1} was observed for the thin film of Co_3O_4, at a charge–discharge current density of 2.5 A g^{-1}. To the best of our knowledge, this is the first time to use UV–ozone treatment to convert a cobalt hydroxide thin film to Co_3O_4; the obtained Co_3O_4 thin film shows an excellent specific capacitance. The UV–ozone treatment is fast and simple for the conversion of cobalt hydroxide thin film to Co_3O_4 thin film at a relatively low temperature, and is a promising technique for the low-temperature preparation of nanostructural metal-oxide thin films on flexible substrates.

2. Experimental

2.1. Chemicals

Cobalt nitrate 6-hydrate (A.C.S. reagent, J.T. Baker), ammonium fluoride (A.C.S. reagent, J.T. Baker), nitric acid (65%, Sigma–Aldrich), isopropyl alcohol (99%, Sigma–Aldrich), and sodium hydroxide (A.C.S. reagent, J.T. Baker) were used as received. Deionized water (DIW) was used throughout the work.

2.2. Apparatus

Potentiostatic electrodeposition, cyclic voltammetry (CV), and chronopotentiometric experiments were performed with a CHI 440 electrochemical workstation (CH Instruments, Inc., USA). A conventional three-electrode system was used in all the electrochemical experiments, mentioned above. A polished and cleaned Ti foil was used as the working electrode for the electrodeposition, and the Ti foil modified with the cobalt hydroxide or cobalt oxide was used as the working electrode for the CV and chronopotentiometric experiments. For all experiments, a Pt foil (4.0 cm × 1.0 cm) and an Ag/AgCl/saturated KCl (homemade) were used as the counter and reference electrode, respectively. All electrochemical experiments were performed at room temperature and all the potentials were reported against the Ag/AgCl/sat'd KCl reference electrode.

Nanostructures of the cobalt oxide films were observed by using scanning electron microscope (SEM, Nova NanoSEM 230) and transmission electron microscope (TEM, Hitachi H-7100, Japan). The selected area electron diffraction (SAED) patterns were also obtained by the same TEM apparatus. The structural characterizations of the films of cobalt hydroxide and oxide were verified by X-ray diffraction patterns (XRD, X-Pert, the Netherlands) with Cu K_α radiation. The powder of cobalt oxide scraped from its' film was also characterized by the same XRD apparatus. The compositions of the films of cobalt hydroxide and oxide were verified by X-ray photoelectron spectroscopy (XPS, PHI 5000 VersaProbe system, ULVAC-PHI, Chigasaki, Japan), using a microfocused (100 μm, 25 W) Al X-ray beam, with a photoelectron takeoff angle of 45°. The Ar^+ ion source (FIG-5CE) was controlled by using a floating voltage of 0.2 kV. The Wienfiltered C_{60}^+ ion source (IOG C60-10, Ionoptika, Chandler's Ford, UK) was operated at 10 mA and 10 kV. The binding energies obtained in the XPS analyses were corrected for specimen charging, by referencing the C 1 s peak to 284.60 eV. UV–ozone cleaning machine (Jelight Company, Inc., Model No. 42) was used for the UV–ozone treatment for the thin films, throughout the work.

2.3. Preparation of the flexible Co_3O_4 modified Ti electrode

A flexible Ti foil (0.1 mm, 99.5%) was polished and cleaned first by the following procedure. First, the Ti foil was soaked in a 65% nitric acid solution containing 0.2 M of ammonium fluoride for 15 min, in order to etch the oxidized and contaminated layers on the surface, and was washed by DIW. Thereafter, the Ti foil was soaked and sonicated first in isopropyl alcohol, and then in DIW. The sonicated period for each step was 5 min. After finishing this polishing and cleaning procedure, the Ti foil was used for the deposition of a thin film of Co_3O_4. The thin film was synthesized by a one-step potentiostatic electrodeposition, followed by an UV–ozone treatment. The electrodeposition process was carried out potentiostatically at −1.0 V with respect to an Ag/AgCl/KCl (sat'd) reference electrode. The polished and cleaned flexible Ti foil was used as the working electrode with an exposed area of 0.5 cm^2, and a Pt foil was used as the counter electrode. A solution of 0.10 M cobalt nitrate 6-hydrate was used as the electrolyte for the electrodeposition process. The electrodeposition time was chosen as 4 min. Thereafter, the electrode modified with the electrodeposited film was subjected to the UV–ozone cleaning for 30 min in air. A flexible Ti electrode modified with Co_3O_4 was thus obtained. For comparison, another type of Ti electrode modified with Co_3O_4 was also obtained by annealing the electrodeposited film at 200 °C for 1 h.

2.4. Estimation of mass of the thin films

In order to calculate the specific capacitance of the thin films, the mass of the films were estimated by Faraday's law, on the assumption that Faraday's current efficiency for electrodeposition was 100%. The reactions for the cathodic electrodeposition process in the solution containing nitrate ions have been reported in several literatures and can be expressed as follows [15–18],

$$NO_3^- + H_2O + 2e^- \rightarrow NO_2^- + 2OH^- \quad (1)$$

$$2OH^- + Co^{2+} \rightarrow Co(OH)_2 \quad (2)$$

According to these reactions, the total number of cobalt ions in the electrodeposited film could be calculated from the total charge

used for the electrodeposition process. Thereafter, the mass of the films before and after UV–ozone treatment could be estimated after confirming their chemical formulas.

3. Results and discussion

3.1. Characterization of the films before and after the UV–ozone treatment

Fig. 1(a) and (b) shows photos of the film on flexible Ti substrate before and after the UV–ozone treatment, respectively. The electrodeposited film showed a pale green color before its UV–ozone treatment, and a dark black color after its treatment. The SEM images of the thin film before and after the UV–ozone treatment are shown in Fig. 1(c) and (d), respectively. Both the films show mosaic sheet-like nanostructures. Although the macroscopic colors of the film are quite different, there is no microscopic morphology change in the film before and after UV–ozone treatment.

The XRD patterns of the film before and after UV–ozone treatment are shown in Fig. 2. In addition to the diffraction peaks of Ti substrate, the film obtained before UV–ozone treatment shows three small diffraction peaks of $Co(OH)_2$, located at 10.1, 33.1, and 59.0°, respectively [19]. This observation indicates that the electrodeposited film contains low-crystalline $Co(OH)_2$. The as-prepared thin film, when it is electrodeposited, is known to consist of α-$Co(OH)_2$ and β-$Co(OH)_2$ [16,18,20–22]. The green cobalt hydroxide film was reported to be low-crystalline [18,22], which agrees with our observation. The high concentration of cobalt nitrate in the electrodeposited solution (0.10 M) causes the massive aggregates of cobalt hydroxide, leading to the low-crystalline cobalt hydroxide film [18]. The partial protonation of the $Co(OH)_2$ layers happens during the electrodeposition simultaneously, resulting in the incorporation of positive charge on the layers. This protonation gives rise to the intercalation of NO_3^- and water into the film due to charge neutralization, resulting in the hydrotalcite-like structure of $Co(OH)_2$. This may be the possible reason for the formation of the low-crystalline cobalt hydroxide film with sheet-like morphology. The similar mechanism has been

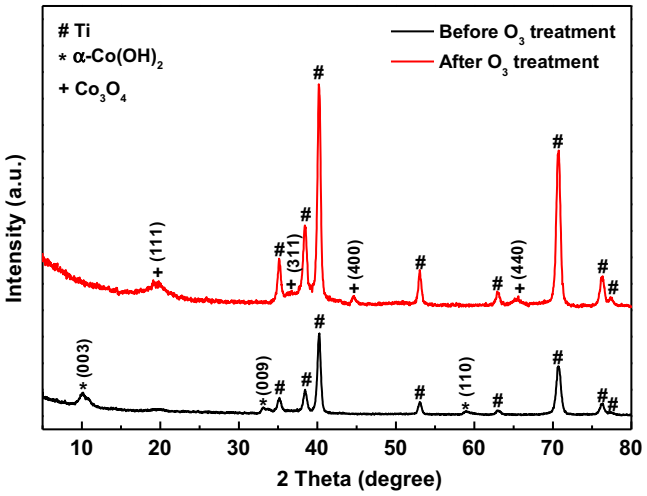

Fig. 2. XRD patterns of the film before and after the UV–ozone treatment.

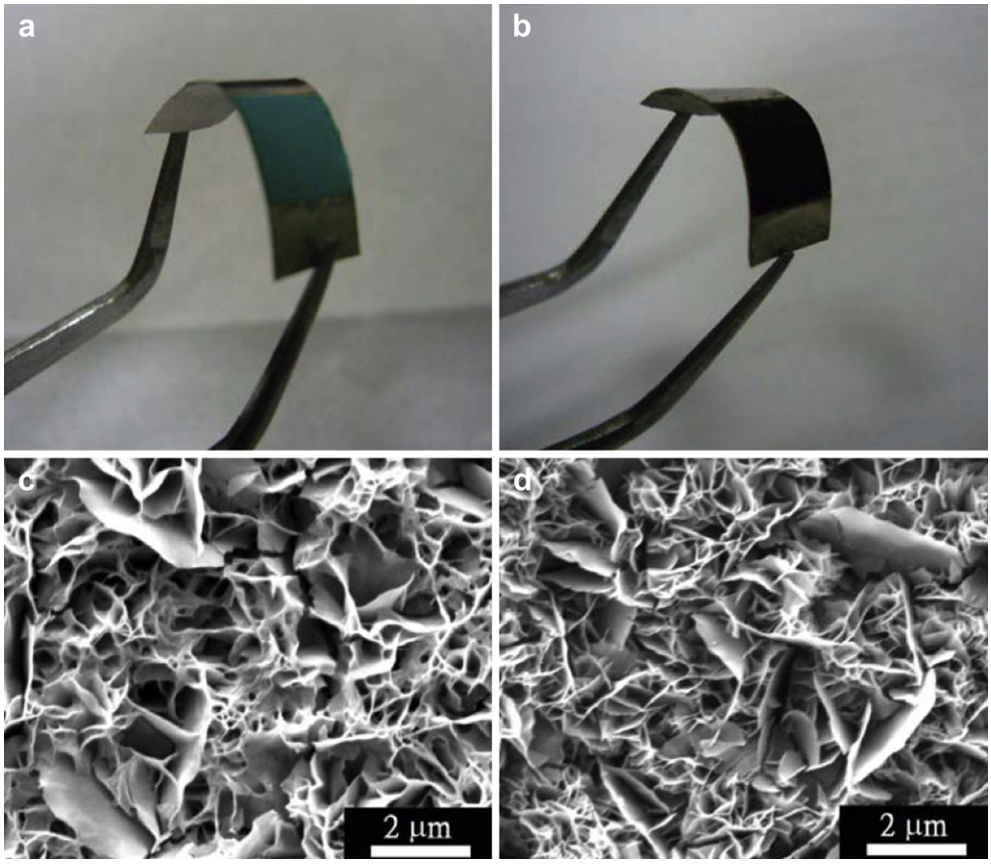

Fig. 1. Photos of the film on a flexible Ti substrate (a) before UV–ozone treatment and (b) after UV–ozone treatment; SEM images of the film (c) before UV–ozone treatment and (d) after UV–ozone treatment.

proposed previously [19,22,23]. The XRD pattern of the Ti foil with the thin film after its UV–ozone treatment also shows the diffraction peaks of Ti substrate. However, in addition to the peaks of Ti substrate, four additional diffraction peaks can be observed. These peaks can be indexed to Co_3O_4, according to Joint Committee on Powder Diffraction Standards (JCPDS, PDF no. 76–1802). The grain size of the Co_3O_4 film was calculated to be 5.3 nm, from the diffraction peak of the (111) plane in its XRD pattern, according to the Scherrer's formula [24],

$$d = \frac{\lambda}{B\cos\theta} \tag{3}$$

where λ and B are the wavelength of X-ray and the full-width at half maximum intensity, respectively. In addition, the film after UV–ozone treatment was also scraped to form powder for the powder XRD measurement, and the result is shown in Fig. S1 in the Supplementary data. The XRD power pattern shows only the diffraction peaks of Co_3O_4, which is in agreement with the result of the thin film XRD pattern (Fig. 2).

Fig. 3(a) and (b) shows the TEM images of the powders scraped from the films before and after UV–ozone treatment, respectively. It can be seen that the TEM image of the film before UV–ozone treatment shows a smooth sheet-like structure, as shown in Fig. 3(a). However, the TEM image of the film after UV–ozone treatment shows a rough nanosheet, which is composed of several tiny nanoparticles (Fig. 3(b)). The SAED patterns of the powders scraped from the films before and after UV–ozone treatment are shown in Fig. 3(c) and (d), respectively. Both results show ring-like patterns, indicating that both films are polycrystalline.

To further confirm the composition of the film, XPS analysis was applied for the film before and after UV–ozone treatment. High-resolution XPS spectra in the region of Co 2p for the film before and after UV–ozone treatment are shown in Fig. 4(a) and (b), respectively. The XPS spectrum in Fig. 4(a) shows two peaks with a peak separation of 16 eV and with binding energies at 781.3 and 797.3 eV, corresponding to Co $2p_{3/2}$ and Co $2p_{1/2}$, respectively. These two peaks indicate the presence of β-$Co(OH)_2$ in the electrodeposited film [25,26]. Two more peaks can also be seen with the binding energies at 776.0 and 791.5 eV; to the best of our knowledge, these two peaks were not previously shown in any report. However, previous reports [16,18,20–22] suggest the presence of α-$Co(OH)_2$ in the electrodeposited cobalt hydroxide film (formed before the UV–ozone treatment in our case); therefore we assume that the peaks in our case at 776.0 and 791.5 eV are due to α-$Co(OH)_2$. Fig. 4(b), however, shows only two peaks with a peak separation of 14.8 eV and with binding energies at 779.8 and 794.6 eV, which correspond to the characteristic XPS peaks of Co_3O_4 [1,25,26]. The spectrum in Fig. 4(b) further confirms that the thin film was converted to Co_3O_4 after the UV–ozone treatment. In the following discussions, the modified electrode before the UV–ozone treatment is designated as $Co(OH)_2$/Ti, and the one after the UV–ozone treatment is designated as Co_3O_4/Ti.

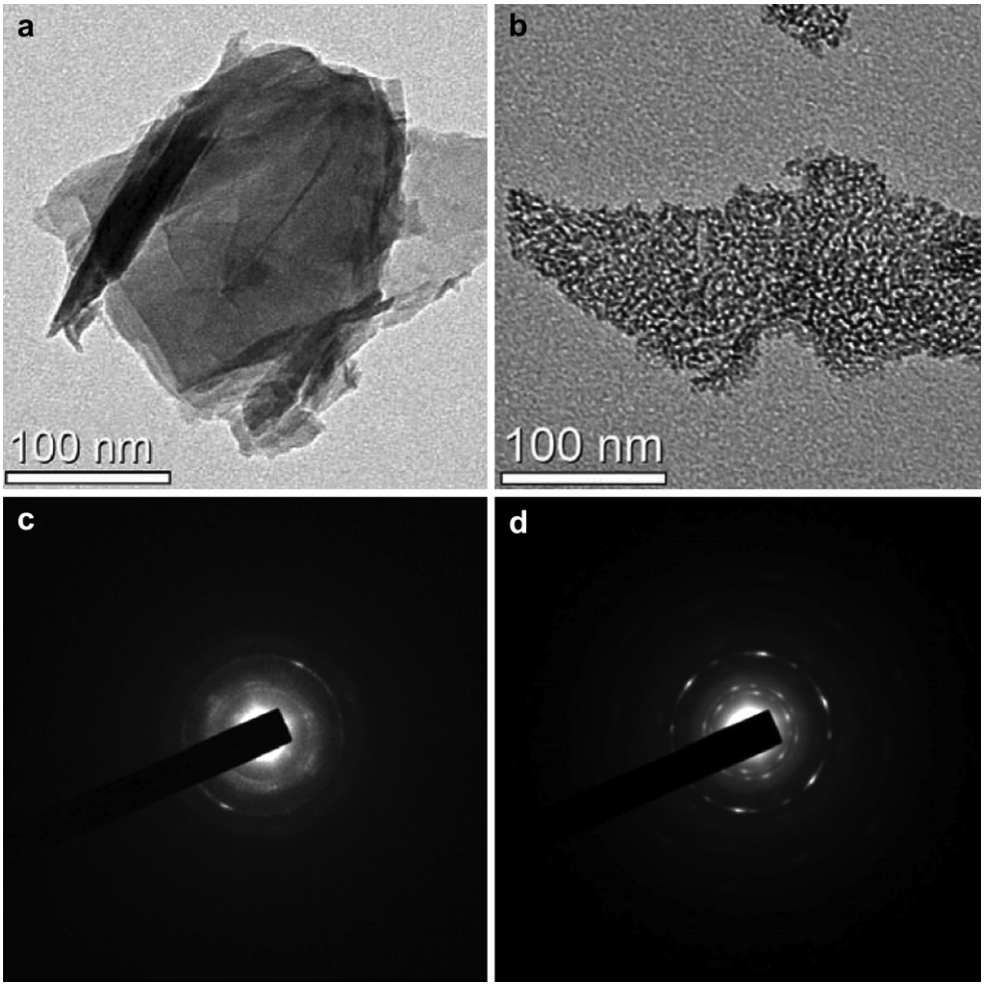

Fig. 3. TEM images of the powders scraped from the films (a) before UV–ozone treatment and (b) after UV–ozone treatment; SAED patterns of the powders scraped from the films (c) before UV–ozone treatment and (d) after UV–ozone treatment.

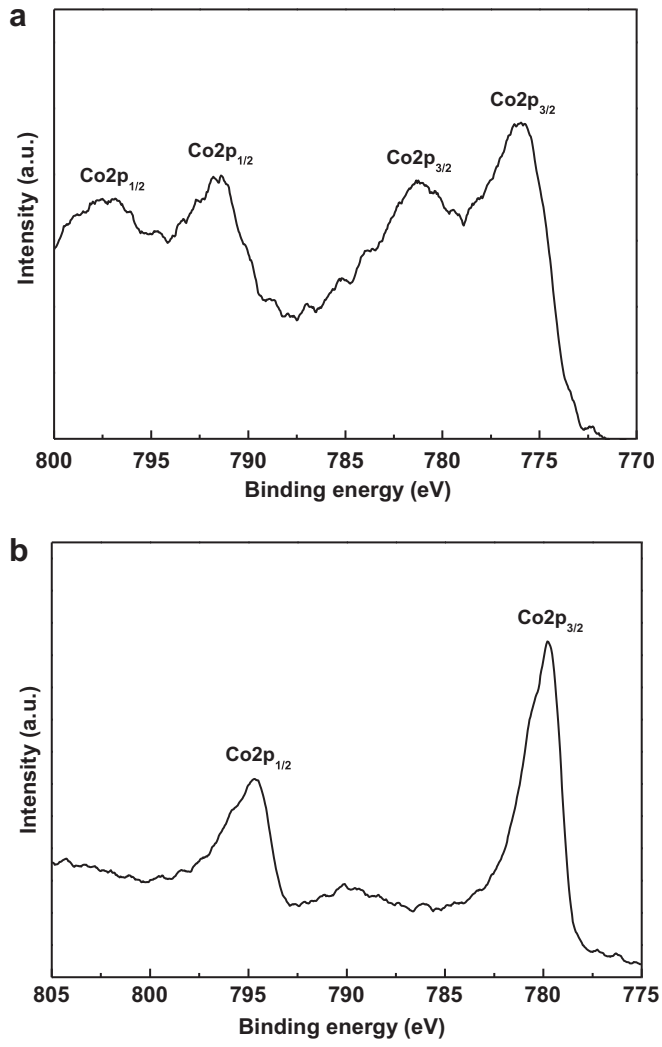

Fig. 4. High-resolution XPS spectra in the region of cobalt element for the film (a) before UV–ozone treatment and (b) after UV–ozone treatment.

3.2. Electrochemical behavior of $Co(OH)_2$/Ti and Co_3O_4/Ti

Fig. 5 shows CV responses of bare Ti substrate, $Co(OH)_2$/Ti, and Co_3O_4/Ti, obtained in 5.0 M NaOH solutions at a scan rate of 25 mV s^{-1}. The electrodes were potential cycled till the CVs became stable and then only the CV curves were recorded. The geometric areas of the bare Ti substrate and the two modified electrodes were fixed to be 0.5 cm^2, for all the following experiments. The bare Ti substrate does not show any redox peaks, as expected. The $Co(OH)_2$/Ti electrode also does not show any perceivable faradic current in its stable CV curve. The CV curve of Co_3O_4/Ti shows a remarkable oxidation peak at about 0.01 V and a reduction peak at about −0.07 V; the CV also shows a pair of hump-like redox peaks at about 0.36 V. The electrochemical redox reactions at the first center (0.01 V and −0.07 V) may be represented as [27–30],

$$Co_3O_4 + OH^- + H_2O \rightarrow 3CoO(OH) + e^-, \quad (4)$$

and the redox reactions at the second center (at about 0.36 V) may be represented as,

$$CoO(OH) + OH^- \rightarrow CoO_2 + H_2O + e^-. \quad (5)$$

The CV curve of Co_3O_4/Ti shows much larger enclosed area than the other two CVs, implying much better capacitor performance of

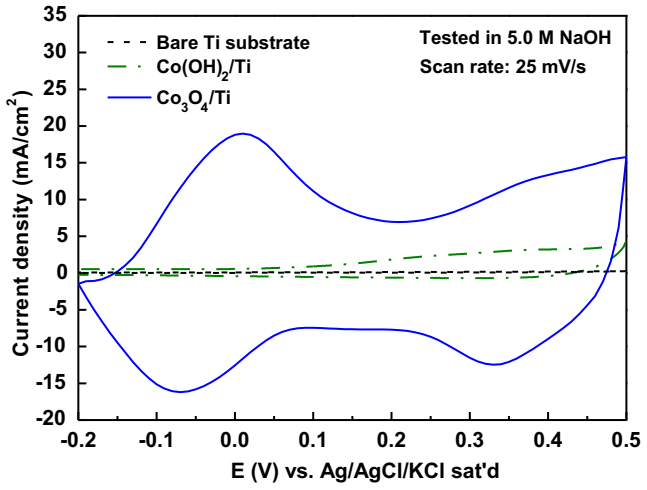

Fig. 5. Cyclic voltammetric responses of bare Ti substrate, $Co(OH)_2$/Ti, and Co_3O_4/Ti, obtained in 5.0 M NaOH solutions, at a scan rate of 25 mV s^{-1}.

Co_3O_4/Ti than those of the other two electrodes. Besides, the enclosed area of CV curve of the Ti substrate is insignificant, with reference to that of Co_3O_4/Ti, indicating the excellent capacitor behavior of Co_3O_4/Ti, which is obviously due to the Co_3O_4 thin film.

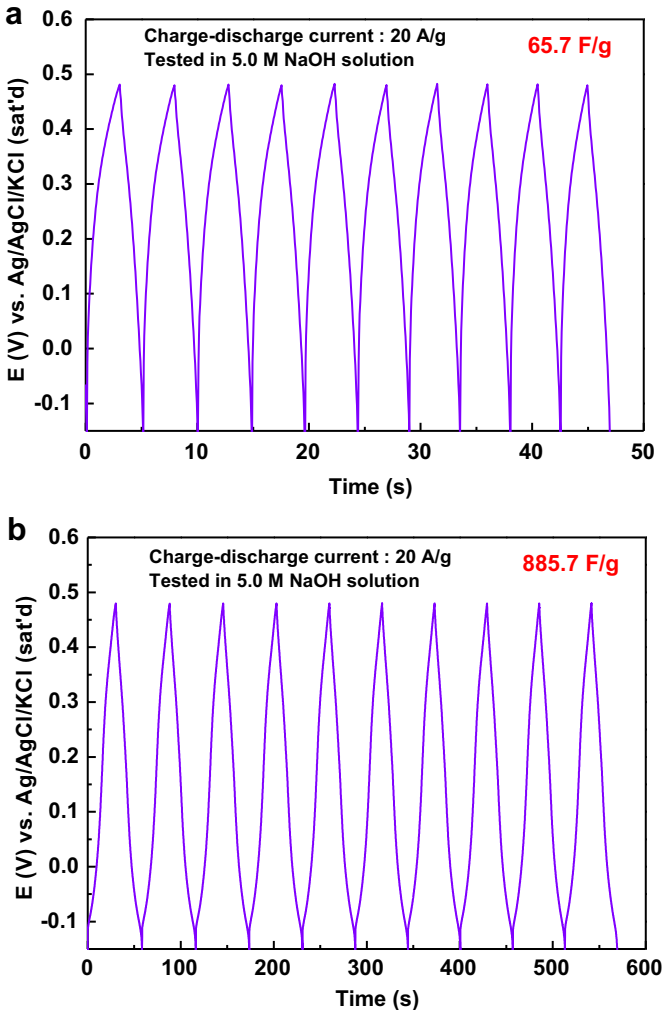

Fig. 6. Charge–discharge curves of (a) $Co(OH)_2$/Ti and (b) Co_3O_4/Ti, obtained in 5.0 M NaOH solutions with a charge–discharge current of 20 A g^{-1}.

With reference to electrochemical pseudocapacitors, the charge and discharge processes of Co_3O_4 are attributed to these two redox reactions, i.e., reactions (4) and (5). Thus, chronopotentiometric measurements were made on Co_3O_4/Ti, in order to construct a charge–discharge curve, and thereby to calculate the film's specific capacitance for the modified electrode. To discuss the difference in specific capacitances of the film before and after its UV–ozone treatment, $Co(OH)_2$/Ti was also subjected to the same chronopotentiometric measurement. The electrolyte was chosen to be a 5.0 M NaOH, the charge–discharge current density was 20 A g^{-1}, and the potential range was from −0.15 V to 0.48 V. The charge–discharge curves of $Co(OH)_2$/Ti and Co_3O_4/Ti are shown in Fig. 6(a) and (b), respectively. After estimating the mass of the film from the charge of the electrodeposition process, the specific capacitance was calculated, by using the following equation [2,8,9],

$$C = \frac{i \times t_d}{\Delta V \times m} \quad (6)$$

where C is the specific capacitance, t_d is the discharge time measured from the charge–discharge curve, i is the charge–discharge current, ΔV is the width of the potential range, and m is the estimated mass of the film. Fig. 6(b) shows a specific capacitance of 885.7 F g^{-1} for the film of Co_3O_4/Ti, which is more than ten times higher than that of $Co(OH)_2$/Ti (65.7 F g^{-1}), both values being obtained at a charge–discharge current density of 20 A g^{-1}. This result indicates that the thin film shows far higher capacitor performance after its UV–ozone treatment, compared to that before its treatment.

The poor capacitor performance of $Co(OH)_2$/Ti is attributed to the irreversible redox property of the low-crystalline $Co(OH)_2$ film. The CV curves of $Co(OH)_2$/Ti for the first and the second cycle of scan in 5.0 M NaOH were recorded and shown in Fig. S2 in the Supplementary data. It can be observed that there are two apparent anodic peaks in the first-cycle CV curve, but no cathodic peak can be observed. It implies that the low-crystalline $Co(OH)_2$ film can be oxidized, but the reaction is totally irreversible. Thus, the CV curve was observed to be stable after the second cycle of scan, but there was no redox peaks observed in the stable CV curve. After the initial cycle, the $Co(OH)_2$/Ti shows only the double-layer capacitance under the repeated charge–discharge cycles, which result in the poor capacitor performance. The irreversible redox property may be attributed to the instability of the non-stoichiometric and low-crystalline $Co(OH)_2$ film, which contains NO_3^- anions intercalated in it.

3.3. Effect of electrodeposition time on the capacitor performance

Various lengths of electrodeposition time, ranging from 3 to 6 min were applied, followed by the same UV–ozone treatment to prepare Co_3O_4/Ti, with various thicknesses of the Co_3O_4 film. Fig. 7(a)–(d) shows the cross-sectional SEM images of the films, prepared for the electrodeposition times of 3, 4, 5, and 6 min, respectively. It can be seen that the film thickness increases from about 4 μm to 6 μm with the increase of electrodeposition time from 3 min to 6 min. The mass of each Co_3O_4 film after UV–ozone treatment was estimated, the charge–discharge curve of each Co_3O_4/Ti was constructed, and the value of specific capacitance of each Co_3O_4 film was calculated. The charge–discharge curves of Co_3O_4/Ti, obtained with different electrodeposition times are shown in Fig. 8(a), and the behaviors of specific capacitance and

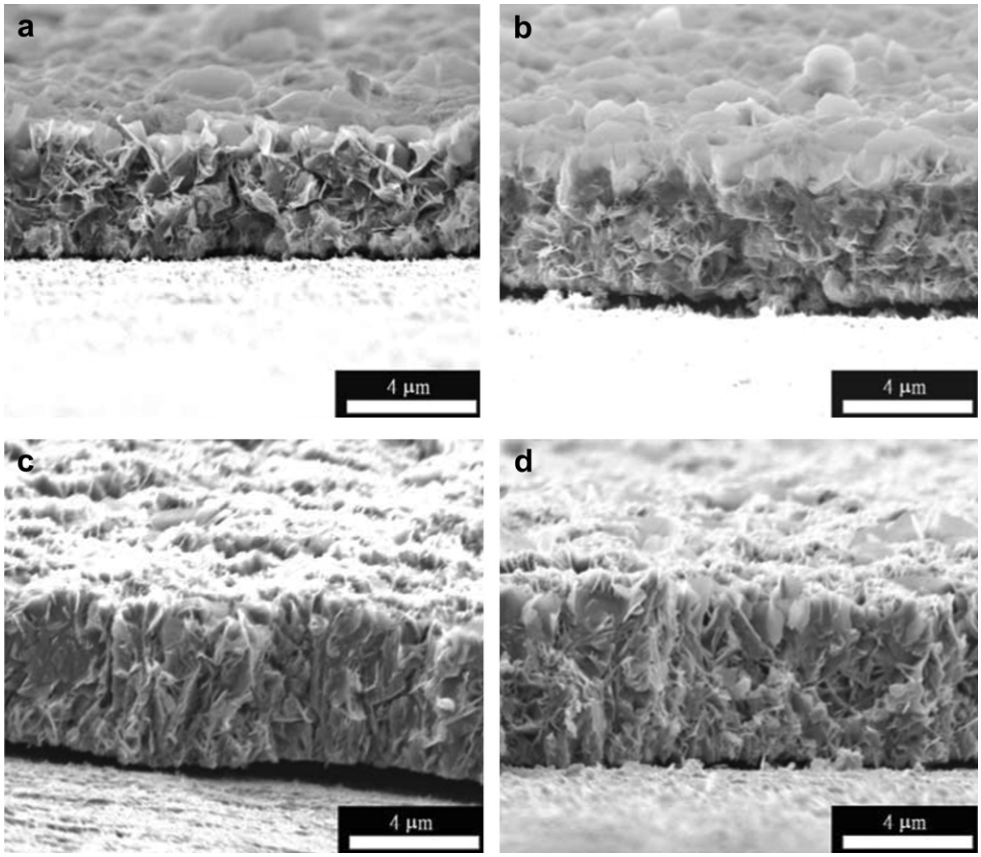

Fig. 7. Cross-sectional SEM images of the films, prepared for the electrodeposition times of (a) 3 min, (b) 4 min, (c) 5 min, and (d) 6 min.

mass of the Co_3O_4 films as functions of the electrodeposition time are shown in Fig. 8(b). All the measurements of capacitance were performed in 5.0 M NaOH solutions, at a charge–discharge current density of 20 A g^{-1}. The mass of the films prepared for the electrodeposition times of 3, 4, 5, and 6 min were estimated to be 0.112, 0.155, 0.179, and 0.217 mg, respectively. It can be seen in Fig. 8(b) that the mass of the film increased continuously, when the electrodeposition time was increased from 3 min to 6 min, but the specific capacitance of the film reached to an optimal level, when the electrodeposited time was 4 min. These behaviors may be explained as follows. When the film thickness increases, the amount of Co_3O_4 used for the charge–discharge process increases, resulting in a higher specific capacitance for the film at this stage. However, when the film becomes too thick, the amount of Co_3O_4 which is effectively available for the charge–discharge process does not increase with the increased film thickness as fast as before, due to the less effective ionic conduction in the bulk film, but the mass of the film still increases with the increased film thickness as usual. According to Eq. (6), the specific capacitance decreases with the increased film thickness at this stage. For all the following experiments, the electrodeposition time for Co_3O_4/Ti was chosen to be 4 min.

3.4. Effect of NaOH concentration in the electrolyte

Solutions of various NaOH concentrations, ranging from 0.1 to 10.0 M, were used as the electrolytes for the chronopotentiometric measurements. Specific capacitance of Co_3O_4 film was measured in each of these electrolytes from the corresponding charge–discharge curve, and the charge–discharge curves of Co_3O_4/Ti in these electrolytes are shown in Fig. 9(a). The charge–discharge current density for all the measurements was 20 A g^{-1}, but the potential range for each measurement was slightly different, due to the pH shift in the electrolyte. Fig. 9(b) shows the specific capacitance of the Co_3O_4 film as a function of concentration of NaOH. It can be seen in Fig. 9(b) that the specific capacitance increases with the increase of the concentration of NaOH up to 5.0 M. This can be easily explained considering Eqs. (4) and (5). A higher concentration of OH^- is more favorable for the oxidation reaction of cobalt oxide; much charge accumulates in the film in the charging process, resulting in a higher capacitor performance. The specific capacitance decreased, when the NaOH concentration increased to 10.0 M; Co_3O_4 thin film, soaked in a solution of 10.0 M NaOH was observed to be destroyed and peeled off from the substrate, because of strong basic nature of the alkali at this concentration.

3.5. Effect of charge–discharge current density

Various charge–discharge current densities were also used for the chronopotentiometric measurements, and the corresponding charge–discharge curves measured in 5.0 M NaOH solution are

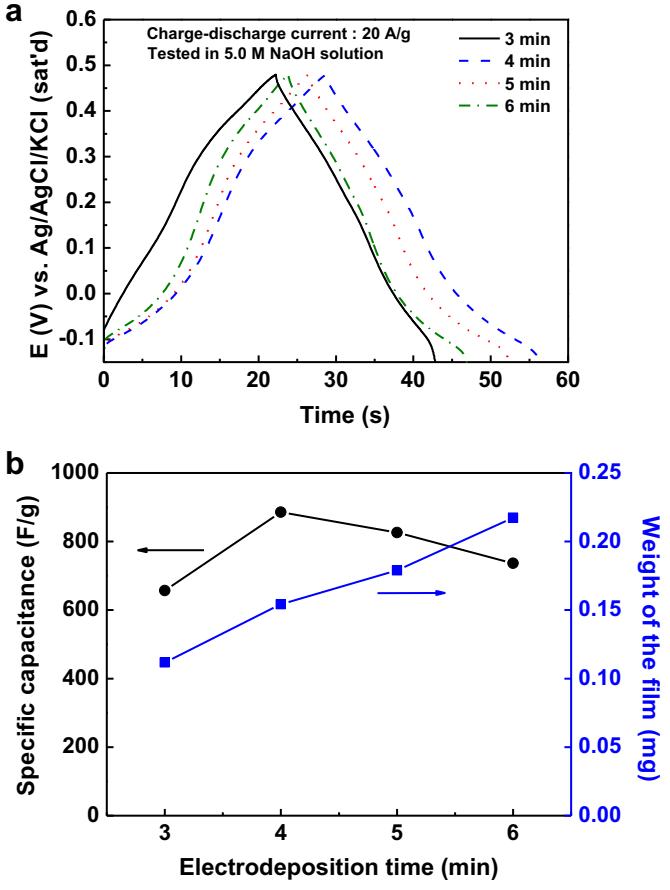

Fig. 8. (a) Charge–discharge curves of Co_3O_4/Ti, obtained with different electrodeposition times, and (b) behaviors of specific capacitance and mass of these Co_3O_4 films as functions of the electrodeposition time. All measurements were performed in 5.0 M NaOH solutions, at a charge–discharge current density of 20 A g^{-1}.

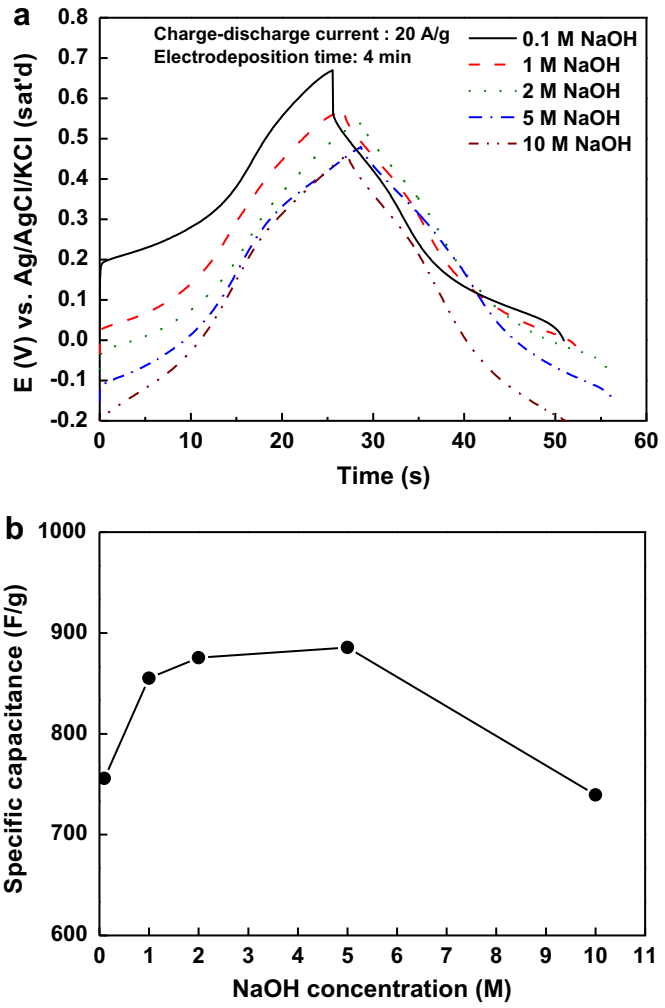

Fig. 9. (a) Charge–discharge curves of Co_3O_4/Ti, measured in various concentrations of NaOH solution, at a charge–discharge current density of 20 A g^{-1}, and (b) specific capacitance of the Co_3O_4 film as a function of concentration of NaOH.

shown in Fig. 10. Fig. 10 shows specific capacitance values of 885.7, 931.6, 986.3, and 1033.3 F g^{-1} for the Co_3O_4 thin film at the charge–discharge current densities of 20, 10, 5, and 2.5 A g^{-1}, respectively. The decrease in specific capacitance at higher charge–discharge current densities may be attributed to the smaller amount of active material involved in the redox reactions.

3.6. Long-term stability

In order to demonstrate the long-term stability of the Co_3O_4/Ti supercapacitor, charge–discharge curve of Co_3O_4/Ti was obtained in 5.0 M NaOH, at a charge–discharge current density of 20 A g^{-1} for 3000 cycles. The plot of specific capacitance (C) versus number of cycles is shown in Fig. 11; charge–discharge curve for the first 20 cycles is shown in the *inset* of Fig. 11. The specific capacitance of the first cycle is designated as C_1, and the values of C/C_1 (%) are also shown in Fig. 11. It can be seen that the value of C/C_1 is still higher than 80% after 2000 cycles of charge–discharge process, and remains at 77% after 3000 cycles. Fig. 11, thus shows the excellent charge–discharge stability of Co_3O_4/Ti, and indicates the high potential of Co_3O_4/Ti for practical supercapacitor applications.

3.7. Effect of crystallinity of the Co_3O_4 film on the capacitor performance

In order to discuss the effect of crystallinity of the Co_3O_4 film on the capacitor performance, another type of Co_3O_4 film was obtained by annealing $Co(OH)_2$/Ti at 200 °C for 1 h. The XRD patterns of $Co(OH)_2$/Ti after UV–ozone treatment (Co_3O_4/Ti) and $Co(OH)_2$/Ti after annealing are shown together in Fig. S3 in the Supplementary data. It can be seen that both patterns exhibit the same XRD peak characteristics, showing the diffraction peaks of Ti and Co_3O_4. However, the peaks intensities for Co_3O_4 are much stronger in the pattern of the film after annealing; this implies the better crystallinity of Co_3O_4 in the annealed film. The charge–discharge curve of the annealed Co_3O_4 film, measured in 5.0 M NaOH at a charge–discharge current of 20 A g^{-1}, is shown in Fig. S4. The specific capacitance of the annealed film is 869.8 F g^{-1}, which is nearly the

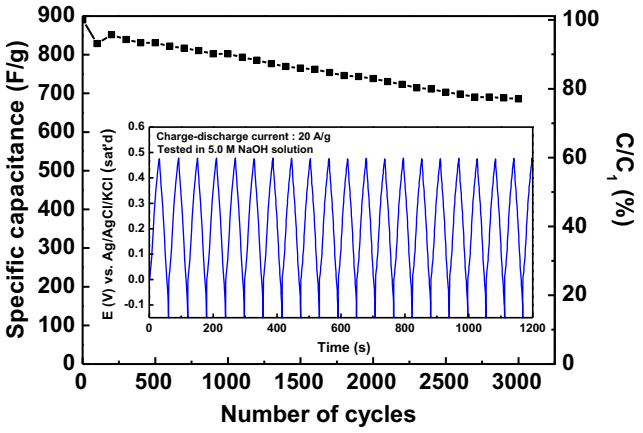

Fig. 11. Specific capacitance of Co_3O_4 film plotted versus number of cycles, obtained in 5.0 M NaOH at a charge-discharge current density of 20 A g^{-1}. Inset: charge–discharge curve for the first 20 cycles.

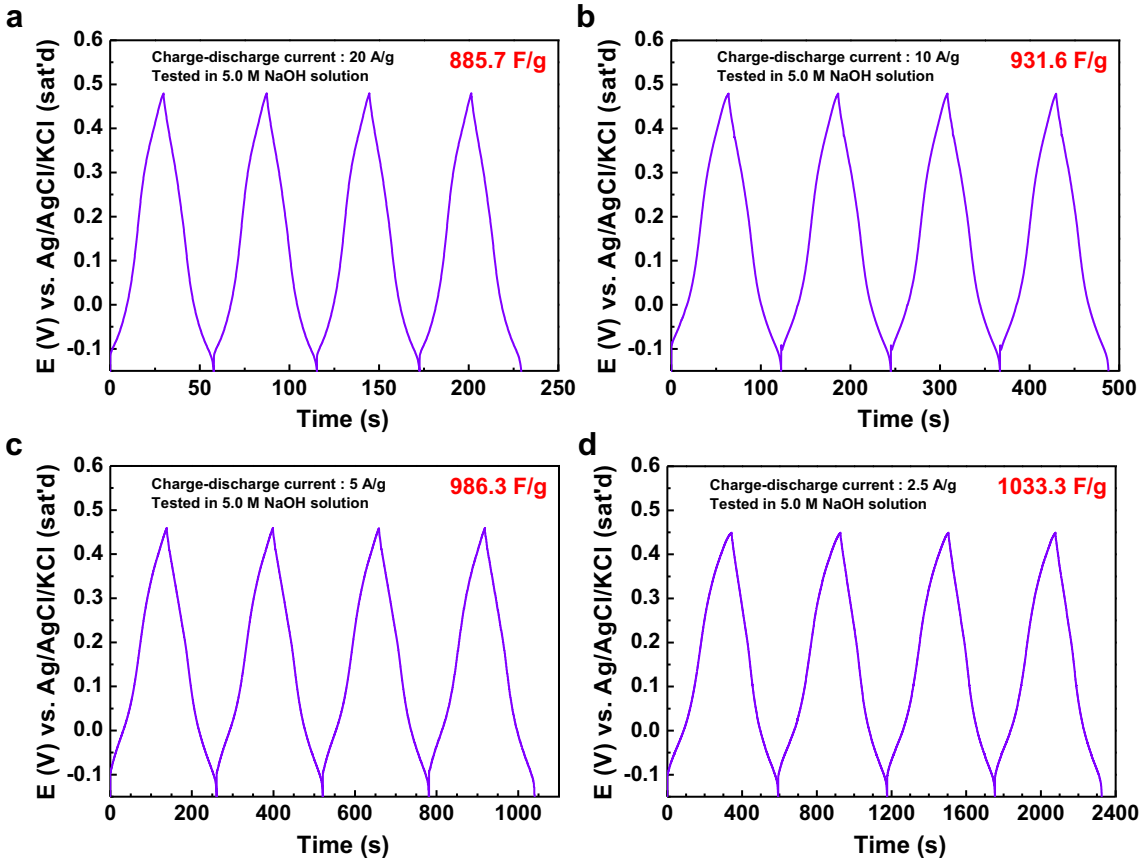

Fig. 10. Charge–discharge curves of Co_3O_4/Ti, measured in 5.0 M NaOH solution, at the charge–discharge current densities of (a) 20 A g^{-1}, (b) 10 A g^{-1}, (c) 5 A g^{-1}, and (d) 2.5 A g^{-1}.

same as Co_3O_4/Ti measured under the same condition (885.7 F/g). This result indicates that the crystallinity of the Co_3O_4 film is not a major factor to affect its' capacitor performance. Co_3O_4/Ti, namely, after UV–ozone treatment, rather than heat treatment, can achieve the excellent capacitor performance even with a lower crystallinity.

4. Conclusions

A thin film of Co_3O_4 was synthesized on a flexible Ti substrate by a one-step potentiostatic electrodeposition, followed by an UV–ozone treatment for 30 min. Both the obtained films, before and after the UV–ozone treatment, were composed of sheet-like nanostructures. No change in the sheet-like morphology was observed before and after the treatment. However, the nanosheets of the film before the UV–ozone treatment were smooth; the nanosheets of the film after the treatment were rough and composed of tiny nanoparticles. The films were verified to be low-crystalline $Co(OH)_2$ and crystalline Co_3O_4 before and after the UV–ozone treatment, respectively. The Co_3O_4 thin film after the UV–ozone treatment showed much better redox activity and capacitor performance than those of the film before the UV–ozone treatment. The specific capacitance of the film of Co_3O_4/Ti was found to be more than ten times higher than that of $Co(OH)_2$/Ti. The electrodeposition time and the NaOH concentration in the electrolyte for the capacitance measurement of the thin film of Co_3O_4 were optimized to be 4 min and 5.0 M, respectively. An excellent specific capacitance of 1033.3 F/g was obtained at a charge–discharge current density of 2.5 A g^{-1}. The data for long-term stability have shown that the specific capacitance of Co_3O_4 has remained to be 77% after 3000 cycles of charge–discharge process. Compared to another type of Co_3O_4 film obtained from annealing, the Co_3O_4 film obtained from UV–ozone treatment, even with a lower crystallinity, shows nearly the same capacitor performance. These findings open up the opportunity for using Co_3O_4/Ti as a high-performance flexible supercapacitor.

Acknowledgments

This work was sponsored by the National Research Council of Taiwan.

Appendix A. Supplementary Material

Supplementary data related to this article can be found online at doi:10.1016/j.jpowsour.2012.04.076.

References

[1] S.L. Xiong, C.Z. Yuan, X.G. Zhang, B.J. Xi, Y.T. Qian, Chem. Eur. J. 15 (2009) 5320–5326.
[2] Y.Y. Gao, S.L. Chen, D.X. Cao, G.L. Wang, J.L. Yin, J. Power Sources 195 (2010) 1757–1760.
[3] J. Xu, L. Gao, J.Y. Cao, W.C. Wang, Z.D. Chen, Electrochim. Acta 56 (2010) 732–736.
[4] S.K. Mondal, N. Munichandraiah, J. Power Sources 175 (2008) 657–663.
[5] Q.H. Huang, X.Y. Wang, J. Li, Electrochim. Acta 52 (2006) 1758–1762.
[6] J. Cheng, G.P. Cao, Y.S. Yang, J. Power Sources 159 (2006) 734–741.
[7] L. Pan, M. Xu, Z.D. Zhang, J. Cluster Sci. 21 (2010) 655–667.
[8] Y.H. Li, K.L. Huang, Z.F. Yao, S.Q. Liu, X.X. Qing, Electrochim. Acta 56 (2011) 2140–2144.
[9] X.X. Qing, S.Q. Liu, K.L. Huang, K.Z. Lv, Y.P. Yang, Z.U. Lu, et al., Electrochim. Acta 56 (2011) 4985–4991.
[10] R.R. Sowell, R.E. Cuthrell, D.M. Mattox, R.D. Bland, J. Vac. Sci. Technol. 11 (1974) 474–475.
[11] J.R. Vig, J. Vac. Sci. Technol. A 3 (1985) 1027–1034.
[12] C.K. Xu, J.M. Wu, U.V. Desai, D. Gao, J. Am. Chem. Soc. 133 (2011) 8122–8125.
[13] M.L. Sham, J.K. Kim, Carbon 44 (2006) 768–777.
[14] J.H. Lee, S.B. Wee, M.S. Kwon, H.H. Kim, J.M. Choi, M.S. Song, et al., J. Power Sources 196 (2011) 6449–6455.
[15] T. Yoshida, D. Komatsu, N. Shimokawa, H. Minoura, Thin Solid Films 451 (2004) 166–169.
[16] M. Dinamani, P. Vishnu Kamath, J. Appl. Electrochem. 30 (2000) 1157–1161.
[17] T. Yoshida, M. Tochimoto, D. Schlettwein, D. Wöhrle, T. Sugiura, H. Minoura, Chem. Mater. 11 (1999) 2657–2667.
[18] J.R.S. Brownson, C. Lévy-Clément, Electrochim. Acta 54 (2009) 6637–6644.
[19] Z.P. Xu, H.C. Zeng, Chem. Mater. 12 (2000) 3459–3465.
[20] T. Yoshino, N. Baba, Solar Energy Mater. Solar Cells 39 (1995) 391–397.
[21] R.S. Jayashree, P. Vishnu Kamath, J. Mater. Chem. 9 (1999) 961–963.
[22] J. Ismail, M.F. Ahmed, P. Vishnu Kamath, J. Solid. State Chem. 114 (1995) 550–555.
[23] P. Vishnu Kamath, G. Helen Annal Therese, J. Solid State Chem. 128 (1997) 38–41.
[24] A. Guinier, X-ray Diffraction in Crystals, Imperfect Crystals, and Amorphous Bodies, Dover Publications, Canada, 1994.
[25] J. Yang, H.W. Liu, W.N. Martens, R.L. Frost, J. Phys. Chem. C 114 (2010) 111–119.
[26] C.V. Schenck, J.G. Dillard, J. Colloid Interf .Sci. 95 (1983) 398–409.
[27] T.R.I. Cataldi, I.G. Casella, E. Desimoni, T. Rotunno, Anal. Chim. Acta 270 (1992) 161–171.
[28] H. Heli, H. Yadegari, Electrochim. Acta 55 (2010) 2139–2148.
[29] E. Hosono, S. Fujihara, I. Honma, M. Ichihara, H.S. Zhou, J. Power Sources 158 (2006) 779–783.
[30] G.I. Casella, M. Gatta, J. Electroanal Chem. 534 (2002) 31–38.